NUMERICAL SIMULATION OF THE BUOYANCY FLOW BETWEEN TWO CONCENTRIC CYLINDERS WITH AZIMUTHAL VARIABLE HEATING

Medina L., Serrano-Aguilera J.J.* and Parras L.
* Author for correspondence
Escuela de Ingenierías, Campus de Teatinos, s/n
University of Málaga,
Málaga, 29071,
Spain,
E-mail: jj.serragui@uma.es

Blanco-Rodríguez F. J.
Área de Mecánica de fluidos,
Departamento de Ingeniería Aerospacial y Mecánica de fluidos
University of Sevilla,
Sevilla, 41002,
Spain

ABSTRACT

In this work, we present novel results of the buoyancy driven flow between two concentric cylinders, when an azimuthal thermal gradient is imposed to the inner cylinder. To accomplish that, angular-dependent temperature distribution (sinusoidal function) is imposed at that surface so that a fourth parameter is added to the problem (Λ). This new parameter accounts for the ratio of amplitude of temperature (amplitude of sinusoidal function) in the inner cylinder to the difference of temperature between the inner and outer cylinder. When this new parameter is zero, one retains the same solutions shown in J.J. Serrano-Aguilera *et al.* [1] (isothermal conditions in both cylinders) but increasing this parameter, the imposed angular gradient in the inner cylinder induces flow structure changes and the subsequent modification in the average equivalent conductivity.

INTRODUCTION

The flow between two concentric cylinders induced by buoyancy is a very well-studied flow experimentally and numerically [2-3]. It has a wide range of applications: from heat exchangers to Concentrated Solar Power Systems (CSP). This is the case of the UVAC receiver in Parabolic Solar Trough Collectors, which are formed by a vacuum annulus to reduce convective thermal losses. When the vacuum is partially lost due to leaks in the sealing between the glass cover and the absorber tube, this sort of flow takes place. Accurate modeling of this phenomenon is of interest since it is responsible for a significant fraction of the total thermal losses. Its simple geometry and well-defined boundary conditions allow to characterize the phenomenon by two dimensionless parameters: the Prandtl number (Pr) which is the ratio of viscous diffusivity to thermal diffusivity and the Rayleigh number (Ra) which can be seen as the ratio of the gravitational potential energy to the energy due to viscous dissipation and thermal diffusion. The aspect ratio $A \equiv D_i/L$ which is the ratio of inner cylinder diameter D_i to the gap width L constitutes the last parameter of the problem.

The basic flow field from the natural convection heat transfer in a horizontal cylindrical annulus for low value of Ra consists of two symmetric crescent-shaped eddies in which fluid rises near the upper surface of the inner hotter cylinder and sinks near the outer colder one. At high Ra, however, several kinds of convective flows which are dependent on Pr and aspect ratio A can be developed. According to Kuehn & Goldstein [4], the flow in a horizontal cylindrical annulus is steady over the range of Rayleigh number from 10^2 to 10^5. Kuehn & Goldstein [2] also experimentally studied the flow patterns at Rayleigh numbers from $2.2 \cdot 10^2$ to $7.7 \cdot 10^7$, and they found that the plume above the inner cylinder began to oscillate when Rayleigh number was near $2 \cdot 10^5$ and the entire plume was turbulent at $Ra \approx 2 \cdot 10^6$.

NOMENCLATURE

A	[-]	aspect ratio
Ra	[-]	Rayleigh number
Nu	[-]	Nusselt number
T	[K]	temperature
$\mathbf{f}_m$	[N/kg]	mass force
$\mathbf{u}$	[m/s]	velocity field
$\mathcal{R}$	[-]	cylinder radius ratio
k	[W/(m·K)]	thermal conductivity
R	[m]	radius
D	[m]	diameter
L	[m]	gap length
g	[m/s^2]	gravitational acceleration
r	[m]	radial coordinate

Special characters

α	[m^2/s]	thermal diffusivity
β	[1/K]	thermal volumetric expansion coefficient
∇	[-]	differential operator nabla
Ψ	[m^2/s]	stream function
Φ	[K]	temperature field with homogeneous boundary conditions
ρ	[kg/m^3]	density
Λ	[-]	amplitude of the variation of temperature on the inner cylinder
ξ	[-]	radial variable in the Chebyshev original domain
θ	[-]	angular coordinate

Subscripts

BC	Boundary Conditions
B	Boussinesq
eq	equivalent
H	hydrostatic
i	inner
o	outer
j	iteration index

Superscripts

$\hat{}$	dimensionless form
$\bar{}$	average

Their results also showed that the local heat transfer coefficient depended significantly on the eccentricity while the overall heat transfer coefficients changed by less than 10% with the change of eccentricity. Yoo [5] in his outstanding work, reported the occurrences of dual solutions at Ra larger than a critical value. Using a vorticity-streamfunction formulation, he observed dual steady solutions at $Ra > Ra_{crit} \approx 3800$ for wide gap annuli ($A = 2$). Similar results were provided later by Mizushima *et al.* [6,7], Xin *et al.* [8], and Mercader *et al.* [9].

Recently, a comprehensive study of the steady solutions of the buoyant flow between isothermal heated cylinders and their global stability has been carried out [1]. Different solutions have been obtained including regions of the parameter space (*Ra-Pr*) where the flow presents two different solutions, with one or multiple plumes.

The aforementioned results can be applied to the comprehension of the underlying mechanisms of the existing heat losses in Parabolic Trough Collectors. As a result of the concentrated solar radiation pattern around the absorber tube, isothermal boundary conditions are not fully realistic in this application. The bottom half of the absorber receives most of the concentrated radiation reflected by the parabolic mirror, which induces thermal gradients around the absorber (inner cylinder). This pattern causes a thermal distribution which can be approximated with a sinusoidal function, whose maximum value is located at the bottom ($\theta = \pi$) of the absorber tube.

GOVERNING EQUATIONS

The problem of buoyancy (gravitational) induced motion of a fluid in a two-dimensional annulus is formulated using the Boussinesq approximation to solve the governing equations of mass, momentum and energy. Note that in the Boussinesq approximation, density variations are assumed to have a fixed part and another part that has a linear dependence on temperature:

$$\rho_B(T) = \rho\left[1-\beta\left(T-T_o\right)\right], \tag{1}$$

where T is the temperature at a point within the fluid, β the thermal volumetric expansion coefficient and T_o is the temperature of the outer cylinder. Fig. 1 shows the geometry of the problem along with the polar coordinate system adopted in which the radial coordinate r is measured from the center of the system and θ is measured clockwise from the upward vertical line. Moreover, the radial velocity u is positive radially outwards and the angular velocity v is positive in the clockwise direction.

The governing equations for the natural convection in the region between horizontal concentric cylinders for an incompressible fluid can be written as

$$\nabla\cdot\mathbf{u} = \mathbf{0}, \tag{2}$$

$$\frac{D\mathbf{u}}{Dt} = -\frac{1}{\rho}\nabla p + \nu\nabla^2\mathbf{u} + \frac{\rho_B(T)}{\rho}\mathbf{f}_m, \tag{3}$$

$$\frac{DT}{Dt} = \alpha\nabla^2 T. \tag{4}$$

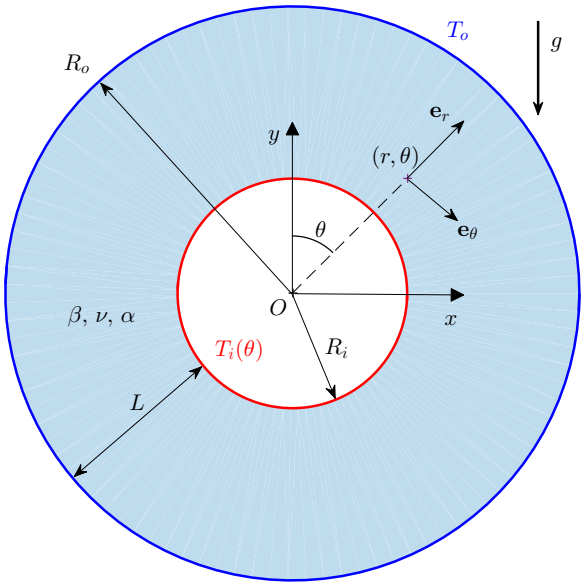

Figure 1: Sketch of the problem.

where ν is the kinematic viscosity, α is the thermal diffusivity, $\mathbf{u} = u(r,\theta)\,\mathbf{e}_r + v(r,\theta)\,\mathbf{e}_\theta$, $\frac{D}{Dt} \equiv \frac{\partial}{\partial t} + \mathbf{u}\cdot\nabla$ is the material derivative and $\mathbf{f}_m$ is the body force per unit mass which corresponds with gravity field for the case the annulus is not rotating.

For the situation in which the fluid is quiescent ($\mathbf{u} = \mathbf{0}$) and at uniform temperature the above equations simplify as

$$-\nabla p_H + \rho\,\mathbf{f}_m = \mathbf{0}. \tag{5}$$

Following the same development as in [3], two equations can be obtained, one for the streamfunction, defined as,

$$\mathbf{u} = \frac{1}{r}\frac{\partial\Psi}{\partial\theta}\,\mathbf{e}_r - \frac{\partial\Psi}{\partial r}\,\mathbf{e}_\theta, \tag{6}$$

and the temperature field $T(r,\theta)$. Furthermore, by setting the characteristic length and velocity of the problem as $l_c = L = R_o - R_i$ and the free-fall velocity $V_f = \sqrt{gL\beta\left(T_i - T_o\right)}$, respectively, and using $\hat{}$ symbol to describe non-dimensional variables, the final non-dimensional equations are:

$$\frac{\partial\hat{\nabla}^2\hat{\Psi}}{\partial\hat{t}} + J\left(\hat{\nabla}^2\hat{\Psi},\hat{\Psi}\right) = \sqrt{\frac{Pr}{Ra}}\,\hat{\nabla}^4\hat{\Psi} + \left[\frac{\cos\theta}{\hat{r}}\frac{\partial\hat{T}}{\partial\theta} + \sin\theta\frac{\partial\hat{T}}{\partial\hat{r}}\right], \tag{7}$$

$$\frac{\partial\hat{T}}{\partial\hat{t}} + J(\hat{T},\hat{\Psi}) = \frac{1}{\sqrt{PrRa}}\hat{\nabla}^2\hat{T}. \tag{8}$$

where $Pr = \frac{\nu}{\alpha}$ and $Ra = \frac{g\beta L^3(T_i-T_o)}{\nu\alpha}$ are the Prandtl and Rayleigh numbers, respectively, $J(\eta,\hat{\Psi}) \equiv \frac{1}{\hat{r}}\left(\frac{\partial\hat{\Psi}}{\partial\theta}\frac{\partial\eta}{\partial\hat{r}} - \frac{\partial\hat{\Psi}}{\partial\hat{r}}\frac{\partial\eta}{\partial\theta}\right)$ represents

the convective term and $\hat{\omega} = -\hat{\nabla}^2\hat{\Psi}$ is the dimensionless axial vorticity.

The boundary conditions on the two impermeable isothermal walls are given by

$$\hat{\Psi} = \frac{\partial\hat{\Psi}}{\partial\hat{r}} = 0, \quad \hat{T} = 1 - \Lambda\cos\theta, \tag{9}$$

on the inner cylinder ($\hat{r} = R_i/L$) and

$$\hat{\Psi} = \frac{\partial\hat{\Psi}}{\partial\hat{r}} = 0, \quad \hat{T} = 0, \tag{10}$$

on the outer cylinder ($\hat{r} = R_o/L$). The dimensional inner cylinder temperature is $T(\theta) = T_i - \Delta T\cos(\theta)$ and on the exterior cylinder is fixed to $T = T_o$ so the parameter Λ is defined as $\Lambda = \Delta T/(T_i - T_o)$.

In case symmetry with respect to the y-axis is imposed, where only half of the annulus is taken as the computational domain, the following symmetric condition is applied along two vertical lines of symmetry at $\theta = 0$ and $\theta = \pi$:

$$\hat{\Psi} = \frac{\partial\hat{\Psi}}{\partial\theta} = \frac{\partial\hat{T}}{\partial\theta} = 0. \tag{11}$$

The solution of the heat equation with the same boundary conditions (which is only function of the radial coordinate) is an important reference to measure heat transfer efficiency of natural convection process. Therefore, in order to measure the convergence of the system and compare our solutions with those provided by other authors [1], the local and average equivalent conductivity [10] are defined as follows:

$$k_{eq}(\hat{r},\theta) \equiv \frac{Nu}{Nu_c} = -\hat{r}\ln(\mathcal{R})\frac{\partial\hat{T}}{\partial n}, \tag{12}$$

$$\bar{k}_{eq}(\hat{r}) \equiv \frac{\oint k_{eq}(\hat{r},\theta)\,ds}{2\pi\hat{r}} = \frac{-\ln(\mathcal{R})}{2\pi}\oint\frac{\partial\hat{T}}{\partial n}\,ds, \tag{13}$$

where $Nu_c \equiv \frac{1}{\ln(\mathcal{R})}$ is the Nusselt number corresponding to the pure conductive flow and $\mathcal{R} = \frac{R_o}{R_i} = 1 + 2\frac{L}{D_i} = 1 + \frac{2}{A}$ is the radius ratio. According to the geometric configuration we are dealing with ($\frac{\partial\hat{T}}{\partial n} = \frac{\partial\hat{T}}{\partial r}$ and $ds = r\,d\theta$), the above equation can be further reduced to

$$\bar{k}_{eq,i} = \frac{-\ln(\mathcal{R})}{2\pi(\mathcal{R}-1)}\int_0^{2\pi}\frac{\partial\hat{T}}{\partial\hat{r}}d\theta. \tag{14}$$

for the inner cylinder ($\hat{r} = \frac{R_i}{L}$), and

$$\bar{k}_{eq,o} = \frac{-\mathcal{R}\ln(\mathcal{R})}{2\pi(\mathcal{R}-1)}\int_0^{2\pi}\frac{\partial\hat{T}}{\partial\hat{r}}d\theta. \tag{15}$$

for the outer cylinder ($\hat{r} = \frac{R_o}{L}$).

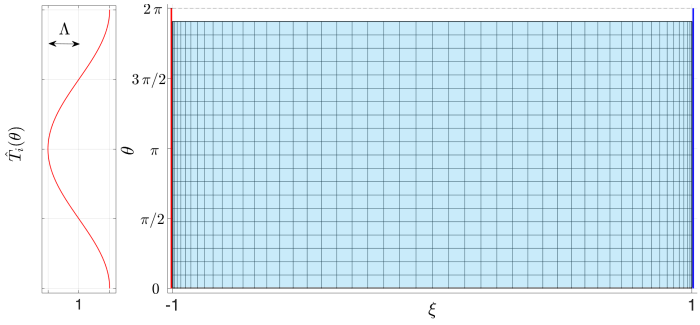

Figure 2: Grid of the numerical domain and boundary condition for the dimensionless temperature field imposed at the hot surface.

Fig. 2 shows the computational grid used for solving the problem where periodic boundary condition is employed in the azimuthal direction, θ. Additionally, Chebyshev discretization allows to radially concentrate the nodes near the walls ($\xi = \pm 1$) in order to accurately solving both the thermal and velocity boundary layers.

NUMERICAL METHOD

We perform a spectral numerical method for the spatial variables using Chebyshev and Fourier discretizations for the radial and azimuthal variables, respectively. Boundary conditions are directly implemented in the derivation matrices using the DM suite toolbox [11].The dimensionless radial domain ($\hat{r} \in [R_i/L, R_o/L]$) is mapped (see Fig. 2) in the Chebyshev domain ($\xi \in [-1, 1]$) using the following path

$$\hat{r} = \frac{1}{2}(\xi+1) + \frac{R_i}{L} = \frac{1}{2}(\xi+1) + \frac{A}{2} \quad \rightarrow \quad \xi = 2\hat{r} - (A+1). \tag{16}$$

Since the derivation matrices implemented in the DM suite require Dirichlet boundary conditions for the temperature, we have decomposed the temperature field as

$$\hat{T}(\hat{r},\theta,\hat{t}) = \hat{\Phi}(\hat{r},\theta,\hat{t}) + \hat{T}_{BC}(\hat{r},\theta) = \hat{\Phi}(\hat{r},\theta,\hat{t}) + \left(1 + \frac{A}{2} - \hat{r}\right)(1 - \Lambda\cos\theta). \tag{17}$$

Substituting the above equation in the vorticity and temperature equations (7-8), we obtain

$$\frac{\partial\hat{\nabla}^2\hat{\Psi}}{\partial\hat{t}} + J\left(\hat{\nabla}^2\hat{\Psi},\hat{\Psi}\right) = \sqrt{\frac{Pr}{Ra}}\hat{\nabla}^4\hat{\Psi} + \left[\frac{\cos\theta}{\hat{r}}\frac{\partial\hat{\Phi}}{\partial\theta} + \sin\theta\frac{\partial\hat{\Phi}}{\partial\hat{r}}\right] + \left[\frac{\cos\theta}{\hat{r}}\frac{\partial\hat{T}_{BC}}{\partial\theta} + \sin\theta\frac{\partial\hat{T}_{BC}}{\partial\hat{r}}\right] \tag{18}$$

$$\frac{\partial\hat{T}}{\partial\hat{t}} + J(\hat{\Phi},\hat{\Psi}) + J(\hat{T}_{BC},\hat{\Psi}) = \frac{1}{\sqrt{PrRa}}\left(\hat{\nabla}^2\hat{\Phi} + \hat{\nabla}^2\hat{T}_{BC}\right). \tag{19}$$

The main advantage of the above formulation is that the deviatoric temperature field $\hat{\Phi}$, has homogeneous Dirichlet boundary conditions at both the inner ($\hat{r} = R_i/L$ or $\xi = -1$) and outer (R_o/L or $\xi = 1$) walls. Once defined the vector $\mathbf{q} = [\hat{\Psi}, \hat{\Phi}]^T$, the system of equations to solve can be written as

$$\mathbf{A}\frac{\partial \mathbf{q}}{\partial \hat{t}} + \mathbf{F}_1(\hat{t},\mathbf{q}) + \sqrt{\frac{Pr}{Ra}}\mathbf{F}_2(\hat{t},\mathbf{q}) + \frac{1}{\sqrt{PrRa}}\mathbf{F}_3(\hat{t},\mathbf{q}) = \mathbf{f}_1(\hat{t},\mathbf{q}) + \frac{1}{\sqrt{PrRa}}\left[\mathbf{f}_2(\hat{t},\mathbf{q}) + \Lambda\mathbf{f}_3(\hat{t},\mathbf{q})\right] + \Lambda\mathbf{f}_4(\hat{t},\mathbf{q}) \quad (20)$$

with

$$\mathbf{A} = \begin{pmatrix} \hat{\nabla}^2 & 0 \\ 0 & 1 \end{pmatrix}, \quad (21)$$

$$\mathbf{F}_1(\hat{t},\mathbf{q}) = \frac{1}{\hat{r}}\begin{pmatrix} \frac{\partial\hat{\Psi}}{\partial\theta}\frac{\partial\hat{\nabla}^2\hat{\Psi}}{\partial\hat{r}} - \frac{\partial\hat{\Psi}}{\partial\hat{r}}\frac{\partial\hat{\nabla}^2\hat{\Psi}}{\partial\theta} \\ \frac{\partial\hat{\Psi}}{\partial\theta}\frac{\partial\hat{\Phi}}{\partial\hat{r}} - \frac{\partial\hat{\Psi}}{\partial\hat{r}}\frac{\partial\hat{\Phi}}{\partial\theta} \end{pmatrix} \quad (22)$$

$$\mathbf{F}_2(\hat{t},\mathbf{q}) = \begin{pmatrix} -\hat{\nabla}^4\hat{\Psi} \\ 0 \end{pmatrix} \quad (23)$$

$$\mathbf{F}_3(\hat{t},\mathbf{q}) = \begin{pmatrix} 0 \\ -\hat{\nabla}^2\hat{\Phi} \end{pmatrix} \quad (24)$$

$$\mathbf{f}_1(\hat{t},\mathbf{q}) = \begin{pmatrix} \frac{1}{\hat{r}}\cos\theta\frac{\partial\hat{\Phi}}{\partial\theta} + \sin\theta\left(\frac{\partial\hat{\Phi}}{\partial\hat{r}} - 1\right) \\ \frac{1}{\hat{r}}\frac{\partial\hat{\Psi}}{\partial\theta} \end{pmatrix} \quad (25)$$

$$\mathbf{f}_2(\hat{t},\mathbf{q}) = \begin{pmatrix} 0 \\ -\frac{1}{\hat{r}} \end{pmatrix} \quad (26)$$

$$\mathbf{f}_3(\hat{t},\mathbf{q}) = \begin{pmatrix} 0 \\ \frac{\cos(\theta)}{\hat{r}^2}\left(1+\frac{A}{2}\right) \end{pmatrix} \quad (27)$$

$$\mathbf{f}_4(\hat{t},\mathbf{q}) = \frac{1}{\hat{r}}\begin{pmatrix} \cos\theta\sin\theta\left(1+\frac{A}{2}\right) \\ -\cos\theta\frac{\partial\hat{\Psi}}{\partial\theta} + \sin\theta\left(1+\frac{A}{2}-\hat{r}\right)\frac{\partial\hat{\Psi}}{\partial\hat{r}} \end{pmatrix} \quad (28)$$

Steady solver

To obtain the steady solution $[\hat{\Psi}_s, \hat{\Phi}_s]^T$ of Eq.(20), a Newton-Raphson solver has been implemented as

$$\mathbf{q}_{j+1} = \mathbf{q}_j - [\nabla_{\mathbf{q}}\mathbf{f}(\mathbf{q}_j)]^{-1}\mathbf{f}_j = \mathbf{q}_j - [\mathbf{B}(\mathbf{q}_j) + \Lambda\mathbf{B}_\Lambda(\mathbf{q}_j)]^{-1}\mathbf{f}_j,$$

where

$$\mathbf{B} = \begin{pmatrix} B_{11} & B_{12} \\ B_{21} & B_{22} \end{pmatrix}, \quad (29)$$

$$\mathbf{B}_\Lambda = \frac{1}{\hat{r}}\begin{pmatrix} 0 & 0 \\ -\cos\theta\frac{\partial}{\partial\theta} + \sin\theta\left(1+\frac{A}{2}-\hat{r}\right)\frac{\partial}{\partial\hat{r}} & 0 \end{pmatrix} \quad (30)$$

$$B_{11} = -\frac{1}{\hat{r}}\left(\frac{\partial\hat{\Psi}_j}{\partial\theta}\frac{\partial\hat{\nabla}^2}{\partial\hat{r}} + \frac{\partial\hat{\nabla}^2\hat{\Psi}_j}{\partial\hat{r}}\frac{\partial}{\partial\theta} - \frac{\partial\hat{\Psi}_j}{\partial\hat{r}}\frac{\partial\hat{\nabla}^2}{\partial\theta} - \frac{\partial\hat{\nabla}^2\hat{\Psi}_j}{\partial\theta}\frac{\partial}{\partial\hat{r}}\right) + \sqrt{\frac{Pr}{Ra}}\hat{\nabla}^4, \quad (31)$$

$$B_{12} = \frac{1}{\hat{r}}\cos\theta\frac{\partial}{\partial\theta} + \sin\theta\frac{\partial}{\partial\hat{r}}, \quad (32)$$

$$B_{21} = -\frac{1}{\hat{r}}\left(\frac{\partial\hat{\Phi}_j}{\partial\hat{r}}\frac{\partial}{\partial\theta} - \frac{\partial\hat{\Phi}_j}{\partial\theta}\frac{\partial}{\partial\hat{r}} - \frac{\partial}{\partial\theta}\right), \quad (33)$$

$$B_{22} = -\frac{1}{\hat{r}}\left(\frac{\partial\hat{\Psi}_j}{\partial\theta}\frac{\partial}{\partial\hat{r}} - \frac{\partial\hat{\Psi}_j}{\partial\hat{r}}\frac{\partial}{\partial\theta}\right) + \frac{1}{\sqrt{PrRa}}\hat{\nabla}^2, \quad (34)$$

being $\mathbf{f}_j = \mathbf{f}(\hat{t},\mathbf{q}_j)$ and j marks the index for each iteration of the algorithm. It is worth mentioning that the steady solutions have been sought taking advantage of their symmetry (antisymmetric $\hat{\Psi}_s$ and symmetric $\hat{\Phi}_s$) with respect to the vertical axis ($\theta = 0$). It has been implemented by means of folding the differentiation matrices, which has allowed a significant reduction of the required computing resources by solving only within the $\theta \in [0, \pi]$ range. A steady solution is considered converged if $\max(|\mathbf{f}_j|) < 10^{-8}$.

NUMERICAL RESULTS

In order to evaluate the effects of the temperature gradient forced on the inner border, one pair of solutions found by [1] are used. Particularly, located at $Pr = 0.2792$ and $Ra = 7.2025 \cdot 10^4$, this pair of solutions show different values of the average equivalent conductivity ($\bar{k}_{eq}$). One of them, displayed in Fig. 3(b), is stable (S) whilst the second one on Fig. 3(e) is unstable (U). As previously defined, Λ accounts for the amplitude of the sinusoidal function describing the angular evolution of the temperature in the inner boundary. When $\Lambda > 0$, it means that the temperature at the bottom of the inner cylinder is higher than in the upper half. Otherwise, if $\Lambda < 0$, the highest temperature of the inner cylinder is located on the top ($\theta = 0$).

As shown in Fig. 4(a), the dependence between $\bar{k}_{eq}$ and Λ is virtually linear. A set of solutions have been found within the range $\Lambda \in [-1, 0.11]$ where $\Lambda < 1$ leads to a heat transfer enhancement since a higher value in $\bar{k}_{eq}$ is achieved. On the other hand, if positive values of Λ are considered, a reduction in $\bar{k}_{eq}$ is observed. An analogous tendency is displayed in Fig. 4(b) for the unstable steady solution, where a set of solutions have been identified within the range $\Lambda \in [-0.805, 0.805]$. A linear dependency can also be identified withing the left hand-side of the plot ($\Lambda < 0$) whereas the value of $\bar{k}_{eq}$ is stabilized beyond ($\Lambda > 0.2$). Regardless of the case, it has also been verified that the average equivalent conductivity is equal in both radial borders ($\bar{k}_{eq,i} = \bar{k}_{eq,o}$), which proves that the solutions found are steady.

Complementary information can be obtained from Fig. 3. Both stream function and temperature in dimensionless form are

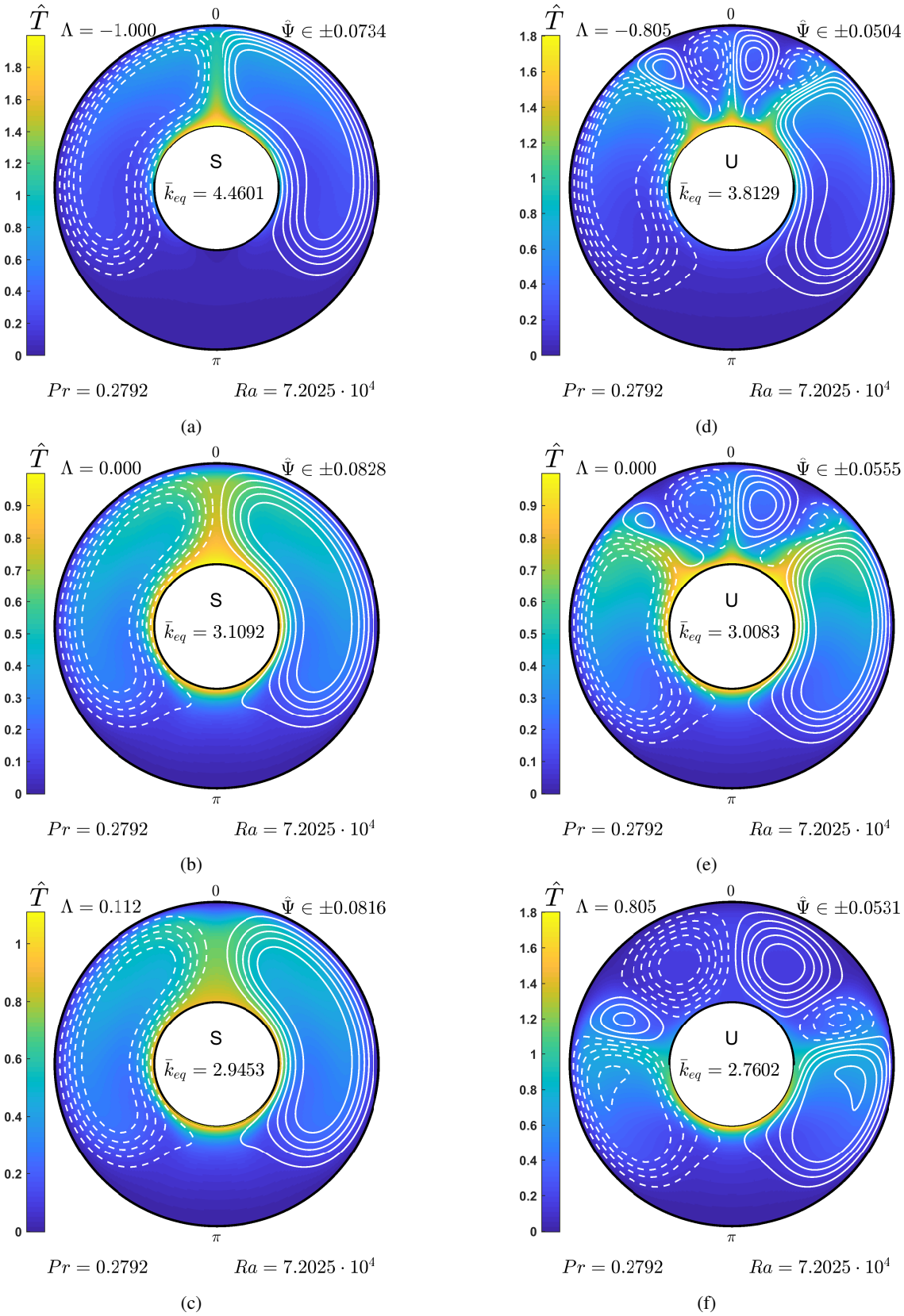

Figure 3: Steady results for the pair of solutions considered as function of the additional parameter Λ. Dimensionless temperature ($\hat{T}$) is displayed in color-scale along with the isocontours of dimensionless stream function ($\hat{\Psi}$).

provided in each subfigure. According to figures 3 (a), (b) and (c), it can be noticed that the angular distribution of temperature in the inner border has a determinant role on the intensity of the upright plume. If higher temperatures are located in the bottom half of the inner cylinder ($\Lambda > 0$), Fig. 3 (c) shows how the vortex intensity is counteracted by the fact that fluid departing from the bottom of the inner cylinder has to circulate around colder parts of the inner border, which leads to a significant reduction on the heat transferred between the inner and outer cylinder. In contrast, subfigure 3 (a) describes a positive impact, where buoyant flow is enhanced, meaning that hot air departing from the hottest point of the inner cylinder directly departs to the outer cylinder.

Similar results can be compiled from the analysis if the Unstable steady solution (figures 3 (d), (e) and (f)), where a concentration of the hottest region in the upper half of the inner cylinder improves heat transfer. However, in this case, it can also be observed an angular shift of the heat plumes. As a matter of fact, if the region of highest temperature is located on the bottom of the inner cylinder ($\theta = \pi$ in Fig. 3 (f)), the main heat plumes are displaced to the bottom half of the fluid domain.

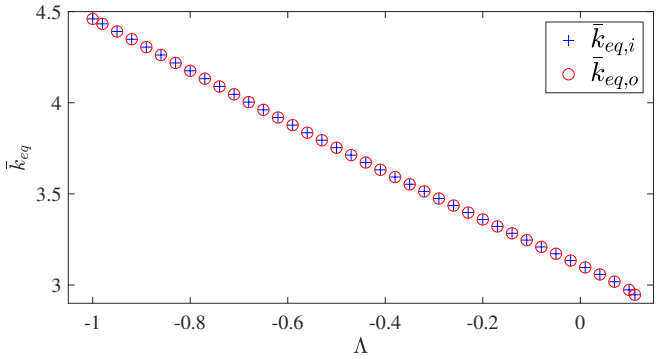

(a) Stable solution

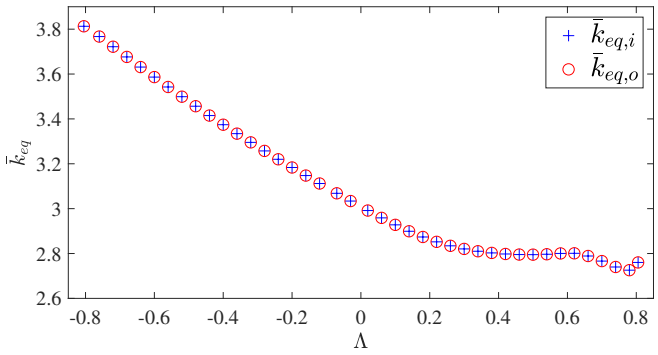

(b) Unstable solution

Figure 4: Dependence of the average equivalent conductivity ($\bar{k}_{eq}$) on the Λ parameter for the Stable steady solution (a) and Unstable steady solution (b).

CONCLUSIONS

The proposed numerical model have already been used and validated to draw a map of solutions in the $Ra - Pr$ space. This work aims to add a fourth parameter (Λ) accounting for the thermal gradients taking place in the absorber tube of a Parabolic Trough Collectors.

It was found that the distribution of temperature around the inner cylinder plays a significant role in the average equivalent conductivity ($\bar{k}_{eq}$). As long as the positive part of the sinusoidal function is located on the upper half of the inner cylinder ($\Lambda < 0$), heat transfer is significantly improved respect to the opposite scenario ($\Lambda > 0$). Not only heat transfer coefficient, but the angular position of the heat plumes are affected by temperature distribution imposed on the inner border, particularly in the case of the unstable steady solution, which shows non-vertical plumes. The dependency $\bar{k}_{eq}$ vs Λ is virtually linear in the negative range of Λ. On the other hand, a nonlinear dependence between these variables has been reported for the unstable steady solution within the positive range of Λ. This fact, could be justified as a result of the significant angular displacement of the plumes.

REFERENCES

[1] Serrano-Aguilera J.J., Blanco-Rodríguez F.J. and Parras L., Global stability analysis of the natural convection between two horizontal concentric cylinders, *International Journal of Heat and Mass Transfer*, (2021), Vol. 172, (2021), pp. 121151

[2] Kuehn H. and Goldstein R.J., An Experimental Study of Natural Convection Heat Transfer in Concentric and Eccentric Horizontal Cylindrical Annuli, *Journal of Heat Transfer*, Vol. 100, (1978), pp. 635-640

[3] Yang X. and Kong S.C., Numerical study of natural convection in a horizontal concentric annulus using smoothed particle hydrodynamics, *Engineering Analysis with Boundary Elements*, Vol. 102, (2019), pp. 11-20

[4] Kuehn T.H. and Goldstein R. J. An experimental and theoretical study of natural convection in the annulus between horizontal concentric cylinders, *Journal of Fluid Mechanics*, Vol. 74, (1976), pp. 695-719

[5] Yoo J.S., Prandtl number effect on bifurcation and dual solutions in natural convection in a horizontal annulus, *International Journal of Heat and Mass Transfer*, Vol. 42, (1999), pp. 3279-3290

[6] Mizushima J. and Hayashi S., Exchange of instability modes for natural convection in a narrow horizontal annulus, *Physics of Fluids*, Vol. 13, (2001), pp. 99-106

[7] Mizushima J., Hayashi S. and Adachi T., Transitions of natural convection in a horizontal annulus, *International Journal of Heat and Mass Transfer*, Vol. 44, (2001), pp. 1249-1257

[8] Xin S. and Le Quéré P., Linear stability analyses of natural convection flows in a differentially heated square cavity with conducting horizontal walls, *Physics of Fluids*, Vol. 13, (2001), pp. 2529-2542

[9] Mercader I., Batiste O., Ramírez-Piscina L., Ruiz X., Rüdiger S. and Casademunt J., Bifurcations and chaos in single-roll natural convection with low Prandtl number, *Physics of Fluids*, Vol. 17, (2005), pp. 104108

[10] Ho-Minh D., Mai D. and Cong Cong T., A Galerkin-RBF Approach for the Streamfunction-Vorticity-Temperature Formulation of Natural Convection in 2D Enclosured Domains, *CMES - Computer Modeling in Engineering and Sciences*, Vol. 44, (2009). Month 04.

[11] Weideman J.A and Reddy S.C., A matlab differentiation matrix suite, ACM Trans. Math. Softw, Vol. 26(4) (2000), pp. 465–519